THE JOURNAL OF BIOLOGICAL CHEMISTRY VOL. 286, NO. 50, pp. 42971–42980, December 16, 2011
© 2011 by The American Society for Biochemistry and Molecular Biology, Inc. Printed in the U.S.A.

Structural Basis for Partial Redundancy in a Class of Transcription Factors, the LIM Homeodomain Proteins, in Neural Cell Type Specification*[S]

Received for publication, April 6, 2011, and in revised form, October 12, 2011 Published, JBC Papers in Press, October 24, 2011, DOI 10.1074/jbc.M111.248559

Morgan S. Gadd[1], **Mugdha Bhati**[1,2], **Cy M. Jeffries, David B. Langley**[3], **Jill Trewhella, J. Mitchell Guss, and Jacqueline M. Matthews**[4]

From the School of Molecular Bioscience, The University of Sydney, New South Wales 2006, Australia

Background: Lhx and Isl proteins contribute to genetic control in developing neurons.
Results: The Lhx3/4-binding motif in Isl2 was identified, and the structures of Lhx-Isl complexes were characterized and compared.
Conclusion: There are minor differences in the structures of Lhx3/4 binding Isl1/2 reflected by mutational and biophysical analyses.
Significance: Redundant sets of interactions conserve function in developing neurons while allowing divergence in other contexts.

Combinations of LIM homeodomain proteins form a transcriptional "LIM code" to direct the specification of neural cell types. Two paralogous pairs of LIM homeodomain proteins, LIM homeobox protein 3/4 (Lhx3/Lhx4) and Islet-1/2 (Isl1/Isl2), are expressed in developing ventral motor neurons. Lhx3 and Isl1 interact within a well characterized transcriptional complex that triggers motor neuron development, but it was not known whether Lhx4 and Isl2 could participate in equivalent complexes. We have identified an Lhx3-binding domain (LBD) in Isl2 based on sequence homology with the $Isl1_{LBD}$ and show that both $Isl2_{LBD}$ and $Isl1_{LBD}$ can bind each of Lhx3 and Lhx4. X-ray crystal- and small-angle x-ray scattering-derived solution structures of an Lhx4·Isl2 complex exhibit many similarities with that of Lhx3·Isl1; however, structural differences supported by mutagenic studies reveal differences in the mechanisms of binding. Differences in binding have implications for the mode of exchange of protein partners in transcriptional complexes and indicate a divergence in functions of Lhx3/4 and Isl1/2. The formation of weaker Lhx·Isl complexes would likely be masked by the availability of the other Lhx·Isl complexes in postmitotic motor neurons.

LIM domains, named for the first three proteins in which the motif was identified (Lin-11/Islet-1/Mec-3), are zinc fingers that coordinate two zinc ions and mediate protein-protein interactions (reviewed in Ref. 1). Two related families of LIM-containing proteins, LIM homeodomain and LIM-only proteins, are expressed in a combinatorial manner along with their protein-binding partners to form the "LIM code," a transcriptional code that helps specify cell type during the development of the central nervous system and many other tissues and organs (*e.g.* Refs. 2 and 3). The 12 mammalian LIM homeodomain proteins comprise six pairs of paralogues (4), which often have overlapping expression patterns and functions. LIM homeobox protein 3 and 4 (Lhx3 and Lhx4)[5] and Islet-1 and -2 (Isl1 and Isl2) are two such paralogous pairs. All four proteins are functional in developing motor neurons (3, 5). Mice in which these genes have been individually disrupted are all embryonic or perinatal lethal, but the phenotypes differ, showing that the pairs of paralogues are not genetically redundant. For example, both $Lhx3^{-/-}$ and $Lhx4^{-/-}$ mice are perinatal lethal but show primary defects in pituitary and lung development, respectively (6, 7). $Isl1^{-/-}$ mice die about halfway through embryonic development (embryonic day 11.5) with abnormal heart and pancreas development and an absence of motor neurons (8), whereas $Isl2^{-/-}$ mice are perinatal lethal, probably due to disrupted breathing resulting from defects in motor neuron differentiation in the thoracic levels of the spinal cord (9).

In differentiating motor neurons, the paralogues show some redundancy. For example, during chick ventral motor neuron development, *Lhx3* and *Lhx4* must both be knocked out to specify dorsal rather than ventral motor neurons (5). In mice and zebrafish, exogenous *Isl1* or *Isl2* can trigger motor neuron differentiation, but both must be expressed to maintain proper motor neuron cell fate (9–11).

Lhx3 and Isl1 form a simple and well characterized example of the LIM code associated with the development of adjacent cell

* This work was supported by grants from the Australian Research Council.
[S] The on-line version of this article (available at http://www.jbc.org) contains supplemental text, Figs. S1–S4, and Tables S1–S4.
The atomic coordinates and structure factors (code 3MMK) have been deposited in the Protein Data Bank, Research Collaboratory for Structural Bioinformatics, Rutgers University, New Brunswick, NJ (http://www.rcsb.org/).
[1] Supported by Australian Postgraduate Awards from the Australian Government.
[2] Present address: School of Biomedical Sciences, Monash University, Victoria 3800, Australia.
[3] Present address: Victor Chang Cardiac Research Institute, Darlinghurst, New South Wales 2010, Australia.
[4] Supported by senior research fellowships from the Viertel Foundation and National Health and Medical Research Council. To whom correspondence should be addressed: Bldg. G08, School of Molecular Bioscience, The University of Sydney, New South Wales 2006, Australia. E-mail: jacqui.matthews@sydney.edu.au.

[5] The abbreviations used are: Lhx3, LIM homeobox protein 3; Lhx4, LIM homeobox protein 4; Isl1, Islet-1; Isl2, Islet-2; Ldb1, LIM domain-binding protein 1; LBD, Lhx3-binding domain; LIM1+2, tandem LIM domains; LID, LIM interaction domain; 3-AT, 3-amino-1,2,4-triazole; λ_{max}, fluorescence emission wavelength maximum; SAXS, small-angle X-ray scattering; r.m.s.d., root mean square deviation.

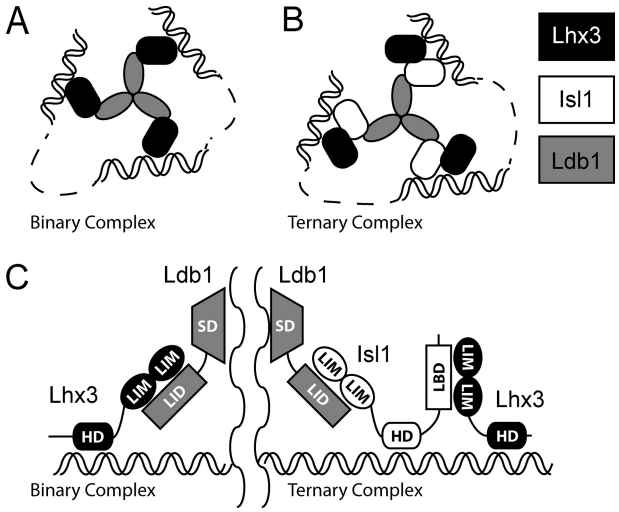

FIGURE 1. **LIM homeodomain complexes in development.** *A*, the proteins Ldb1 (*gray*) and Lhx3 (*black*) assemble into a binary complex. *B*, with the addition of Isl1 (*white*), the ternary complex is preferentially formed (12). Note that the self-association domain of Ldb1 forms trimers *in vitro* (21) and that the homeodomains from Lhx3 and Isl1 bind DNA. The spacing between the homeodomain-binding sites (*dashed lines*) is not defined and may represent close or distant binding sites. *C*, details of domain contacts within the binary and ternary complexes. The LIM interaction domain (*LID*) from Ldb1 makes contacts with the LIM domains (*LIM*) from Lhx3 in the binary complex, but in the ternary complex, $Ldb1_{LID}$ contacts the LIM domains of Isl1, and the LBD from Isl1 binds the LIM domains from Lhx3. *SD*, self-association domain; *HD*, homeodomain.

types (V2 interneurons and motor neurons) in the ventral spinal cord. Lhx3 is expressed in developing V2 interneurons, whereas both Lhx3 and Isl1 are expressed in postmitotic motor neurons. These LIM homeodomain proteins are strong drivers of cell specification. The addition of Lhx3 to dorsal spinal cord cells results in the formation of V2 interneurons, whereas further addition of Isl1 switches their identity to motor neuron cells (12).

Lhx3 and Isl1 form cell-specific transcriptional complexes that also contain LIM domain-binding protein 1 (Ldb1), a widely expressed transcriptional regulator that binds to, and is essential for the activity of, members of the LIM homeodomain and LIM-only families (13–15). Lhx3 binds Ldb1 to generate an active binary complex in V2 interneurons (Fig. 1*A*). In motor neurons, Isl1 disrupts this interaction to form a ternary complex in which Isl1 displaces Lhx3 as the binding partner of Ldb1 and forms additional contacts with Lhx3 (Fig. 1*B*) (12). The contacts between Lhx3 or Isl1 and Ldb1 are made by the tandem LIM domains from the LIM homeodomain proteins and the ~30-residue LIM interaction domain from Ldb1 ($Ldb1_{LID}$) (Fig. 1*C*) (13, 14, 16). An essentially identical interaction is formed between the LIM domains from Lhx3 and an $Ldb1_{LID}$-like sequence near the C terminus of Isl1, the Lhx3-binding domain ($Isl1_{LBD}$) (17).

This study explores the possibility that Isl2 and Lhx4 may be capable of substituting for Isl1 and Lhx3, respectively, in the ternary complex. We identify a new Lhx3-binding domain in Isl2 ($Isl2_{LBD}$), which binds both Lhx3 and Lhx4, and show that $Isl1_{LBD}$ also binds Lhx4. The x-ray crystal structure of $Lhx4_{LIM1+2}$·$Isl2_{LBD}$,[6] combined with biophysical and mutagenic analysis of the series of pairwise interactions, shows that although the structures of Lhx3/4·Isl1/2 pairwise complexes are very similar, there are differences in the nature of the binding interactions between these LIM homeodomain family proteins that likely contribute to diverging biological functions.

[6] Throughout this study, the format Lhx4·Isl2, Lhx3·Isl1, and so forth is used to represent a non-tethered complex or interaction, whereas the format Lhx4-Isl2, Lhx3-Isl1, and so forth is used to represent a tethered protein complex.

EXPERIMENTAL PROCEDURES

Cloning, Mutagenesis, and Protein Expression—The numbering of residues from the proteins refers to the following National Center for Biotechnology Information (NCBI) entries for mouse proteins: Lhx3, P50481; Lhx4, NP_034842; Isl1, NP_067434; Isl2, NP_081673; Ldb1, NP_034827.1. $Lhx3_{LIM1+2}$ refers to residues 28–153, $Lhx4_{LIM1+2}$ refers to residues 24–149, $Isl1_{LBD}$ refers to residues 262–291, $Isl2_{LBD}$ refers to residues 272–301, and $Ldb1_{LID}$ refers to residues 300–330. All clones and mutants were generated by PCR and sequenced to confirm identity (Sydney University Prince Alfred Macromolecular Analysis Centre (SUPAMAC), Royal Prince Alfred Hospital, Sydney, Australia). Constructs of the tethered complexes were generated as described previously (18, 19). All proteins were expressed with a GST tag using pGEX-2T (GE Healthcare) in *Escherichia coli* BL21 (DE3) at 20 °C for 16–20 h. Proteins were purified on glutathione-Sepharose 4B resin (GE Healthcare) and eluted by proteolytic cleavage of the tag with thrombin (Sigma-Aldrich). The proteins were additionally purified by size-exclusion chromatography using a Superdex 200 16/60 column (GE Healthcare).

Protein Characterization—Far-UV CD spectra were collected for samples in 10 mM Tris base (pH 8.5), 150 mM NaF, and 0.5 mM tris(2-carboxyethyl) phosphine at 20 °C as described previously (20). Multi-angle laser light scattering data were collected on samples eluted from a Superose 12 10/30 (GE Healthcare) size-exclusion column as described previously (21).

X-ray Structure Determination and Refinement—The crystallization, collection, and processing of data for Lhx4-Isl2 were described previously (19). The program SOLVE (22) was used with anomalous data to 3.0 Å resolution to identify the zinc atom positions and generate initial phases. Statistical density modification and local pattern matching were carried out using RESOLVE (23). The model was built and revised manually with Coot (24). Refinement of the diffraction data was carried out to 2.16 Å using REFMAC5 and PHENIX with TLS refinement (25–27). The final model was refined using PHENIX. The MOLPROBITY server was used to identify steric clashes and unconventional geometry for validation of the structure (28).

Small-angle X-ray Scattering (SAXS) Data Acquisition and Analysis—Solution SAXS data ($I(q)$ *versus* q, where $q = (4\pi\sin\theta)/\lambda$, 2θ is the scattering angle, and λ the x-ray wavelength) were measured at 10 °C using a SAXSess (Anton Paar) line collimation instrument (10-mm slit width; Ref. 29). For details of sample environments, see supplemental data 3. Data reduction included corrections for beam geometry, sample absorbance, and detector sensitivity as described previously (29). Data were placed on an absolute scale, and the forward scattering at zero angle ($I(0)$) was used to evaluate the molecular weight of the scattering particles (30) using contrast values ($\Delta\rho_M$) and partial specific volumes (υ) derived from the pro-

gram MULCh (31). Guinier analysis of the desmeared data was performed using PRIMUS (32). GIFT (31) was used to calculate probable atom pair distance distributions ($P(r)$ *versus* r) from which the maximum dimension (D_{max}), radius of gyration (R_g), and $I(0)$ of each tethered complex were determined. *Ab initio* shape restorations of the molecular envelopes for each complex were performed using DAMMIF with the outputs from GIFT. Further rigid body modeling was performed using BUNCH (33) (see supplemental data 3 for details). The fits of the refined BUNCH models against the SAXS data were assessed using CRYSOL, which also was used to calculate scattering profiles and fits of the original crystal structures to the data. The $P(r)$ *versus* r of the crystal or BUNCH structures were determined as described in Ref. 34 using GNOM.

Yeast Two-hybrid Analysis—Inserts were cloned into pGAD10 and modified pGBT9 plasmids and co-transformed into AH109 cells (Clontech), as described previously (35). Transformed cells were selected by growth on leucine- and tryptophan-deficient media. For the detection of an interaction, the following selection media were used as indicated (all selection media lacked leucine and tryptophan). For low stringency (−H + X-α-gal), the medium was additionally deficient in histidine (−H) and supplemented with 40 μg ml^{-1} X-α-gal; for moderate stringency (−H + X-α-gal + 3-AT), the medium was as for low stringency but further supplemented with 1 mM 3-amino-1,2,4-triazole (3-AT); for high stringency, the medium was deficient in both histidine and adenine (−H-A). Numbers of yeast cells were normalized such that $A_{600\,nm}$ = 0.2 and were deposited in 2-μl drops at the dilutions indicated.

Chemical Denaturation—Stability studies using guanidine hydrochloride as the denaturant were conducted as described previously (36). Tryptophan fluorescence following excitation at 295 nm was recorded in the range 320–380 nm. The fluorescence emission wavelength maximum (λ_{max}) was used as an indication of the unfolding of the tethered protein complex. The λ_{max} was obtained by fitting of a Gaussian curve through the emission spectra using Origin 6.1 (OriginLab).

RESULTS

Identification of the Lhx3-binding Domain in Isl2—$Isl1_{LBD}$ spans residues 262–291 (Fig. 2*A*) (17). Comparison of the sequences of Isl1 and Isl2 suggested that a similar region in Isl2, residues 272–301 ($Isl2_{LBD}$), might mediate binding to Lhx3 (Fig. 2*A*). We used yeast two-hybrid analysis to test the ability of $Isl1_{LBD}$ and the putative $Isl2_{LBD}$ to interact with the LIM domains of Lhx3 and Lhx4. When the Isl_{LBDs} were fused to the GAL4 DNA-binding domain ($GAL4_{DBD}$), all pairs of proteins exhibited growth on high stringency (−H-A) selection plates, indicating that all four pairwise interactions among these proteins take place (Fig. 2*B*). When the Lhx3/4_{LIM1+2} constructs were fused to the $GAL4_{DBD}$, the Lhx3/4_{LIM1+2}·Isl1/2_{LBD} interactions were all evident under moderate stringency conditions (−H + X-α-gal + 3-AT), and only the interaction between $Lhx4_{LIM1+2}$ and $Isl1_{LBD}$ was detected under high stringency conditions (Fig. 2*C*). Thus, $Isl2_{LBD}$ does mediate interactions with Lhx3, and both Lhx3 and Lhx4 can interact with equivalent domains in Isl1 and Isl2.

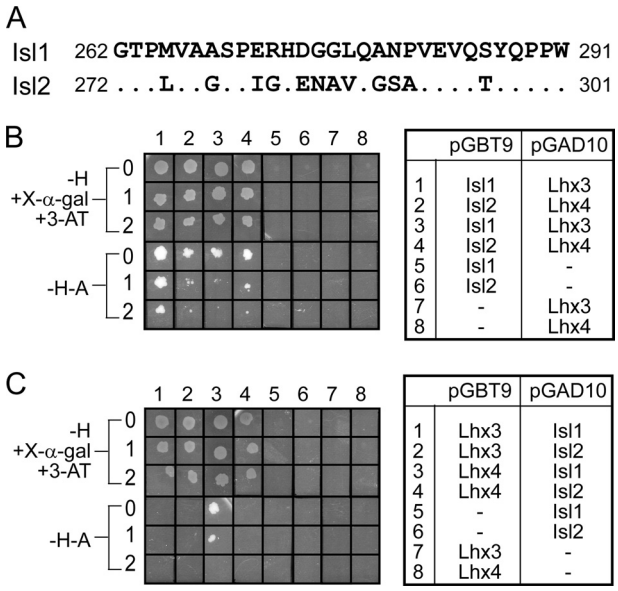

FIGURE 2. **Identification of the Isl2 Lhx3-binding domain, $Isl2_{LBD}$.** *A*, sequence alignment of $Isl1_{LBD}$ and $Isl2_{272–301}$. *Dots* are identical residues. *B* and *C*, pairwise interactions between Isl1/Isl2 and Lhx3/Lhx4 identified by yeast two-hybrid analysis. AH109 yeast cells co-transformed with pGBT9/pGAD10 vectors shown on the *right* were tested for growth under different selection conditions (−H + X-α-gal + 3-AT) or (−H-A); *0* indicates no dilution of yeast cells ($A_{600\,nm}$ = 0.2), *1* indicates a 1:10 dilution ($A_{600\,nm}$ = 0.02), and *2* indicates a 1:100 dilution ($A_{600\,nm}$ = 0.002). pGBT9 encodes the $GAL4_{DBD}$ and pGAD10 encodes the $GAL4_{AD}$.

Generation of Stable Lhx-Isl Constructs—When expressed in bacteria, the LIM domains from Lhx3 and Lhx4, like those from other LIM-only/LIM homeodomain proteins, tend to aggregate and are largely insoluble (37, 38). Tethering an interaction partner such as $Isl1_{LBD}$ or $Ldb1_{LID}$ to the LIM domains protects them from aggregation, allowing soluble tethered complexes to be produced (*e.g.* Refs. 18, 38, and 39). As shown for Lhx4·Isl2 in Fig. 3, *A* and *B*, we generated constructs of the form Lhx3/4_{LIM1+2}-linker-Isl1/2_{LBD}, where the 11-residue linker was designed to be flexible by the inclusion of glycine and serine residues (18, 19). These constructs are subsequently referred to as Lhx3-Isl1, Lhx3-Isl2, Lhx4-Isl1, and Lhx4-Isl2.

All four tethered complexes were monomeric as determined by multi-angle laser light scattering (Fig. 3*C* and supplemental Fig. S1) (17). Far-UV CD spectra of each of the complexes show that the proteins are folded and have similar secondary structure compositions (16–18% helix, 23–26% β-turn, 17–19% β-sheet, and 36–41% coil; Fig. 3*D*).

Crystal Structure of Lhx4-Isl2—The protein Lhx4-Isl2 was crystallized as described previously (19). The structure of Lhx4-Isl2 was determined using single-wavelength anomalous dispersion data recorded at the zinc absorption edge (λ = 1.2819 Å) to a resolution of 2.16 Å (Table 1). The R_{work} and R_{free} are consistent with an x-ray crystal structure of this resolution with some disordered regions (*e.g.* the linker between $Lhx4_{LIM1+2}$ and $Isl2_{LBD}$).

Lhx4 contains two typical LIM domains, each comprising two zinc-coordinating modules made up of two sequential β-hairpins and a short segment of α-helix (Fig. 4*A*, *orange ribbon*). $Isl2_{LBD}$ (*purple ribbon*) binds across the length of both LIM domains, forming a "head-to-tail" complex. $Isl2_{LBD}$ forms

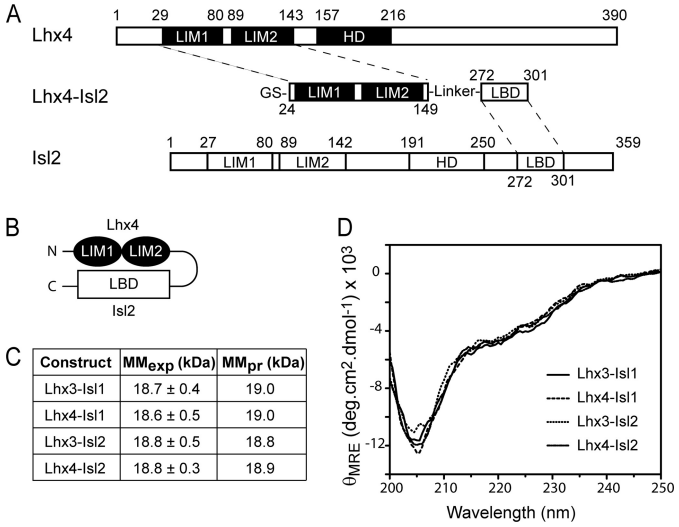

FIGURE 3. **Construction and characterization of the tethered Lhx3/4-Isl1/2 complexes.** *A* and *B*, schematics illustrating the generation of the tethered constructs (*A*) and arrangement of domains (*B*) in the constructs, using Lhx4-Isl2 as an example. *C*, experimental (MM_{exp}) and predicted (MM_{pr}) molecular masses of the complexes as determined by multi-angle laser light scattering. *D*, far-UV CD spectra of the tethered complexes.

TABLE 1

Refinement statistics for Lhx4-Isl2

Values for the highest resolution shell are given in parentheses.

Resolution limit (Å)	2.16 (2.21-2.16)
R_{work} [a]	0.235 (0.294)
R_{free} [b]	0.265 (0.314)
No. of reflections used in refinement	39,191 (2407)
No. of reflections in the test set	2022 (92)
Protein atoms (including zinc)	2201
Solvent molecules	35
r.m.s.d. bond length (Å)	0.003
r.m.s.d. bond angles (°)	0.66
Wilson *B* factor (Å^2)	53
Mean protein *B* factor (Å^2)	58
Mean solvent *B* factor (Å^2)	53
Ramachandran plot, residues in	
Favored regions (%)	95.3
Allowed regions (%)	4.1
Disallowed regions (%)	0.7
Missing side chains [c]	
Common to both chain A and chain B	17
In chain A only	10
In chain B only	4

[a] $R_{work} = \Sigma||F_{obs}| - |F_{calc}||/\Sigma|F_{obs}|$, where F_{obs} and F_{calc} are the observed and calculated structure amplitudes, respectively.
[b] R_{free} is R_{work} for the 5% validation set.
[c] Lists of residues for which there was overall insufficient electron density or that had missing side chains are presented in supplemental Table S2*A* and supplemental Table S2*B*, respectively.

small stretches of β-strand structure along the interface, packing against the second β-hairpin of all four zinc-coordinating modules to make small, three-stranded antiparallel β-sheets.

The two molecules in the asymmetric unit (chains A and B, chain B is shown in Fig. 4*A*) are highly similar (root mean square deviation ~0.28 Å for the backbone atoms). Fourteen residues are missing from both chains, an additional residue is found only in chain A, and another four are found only in chain B. The missing residues are from the linker and termini of the protein (supplemental Table S2*A*). Of the residues modeled, ~20% have missing side chains (see supplemental Table S2*B*), most commonly in the region between the two LIM domains (the "hinge") and the adjacent region in $Isl2_{LBD}$ (the "spacer"). In both chains, residue Asp-66 has poorly defined electron density and lies in the disallowed region of the Ramachandran plot. Apart from these minor differences, both molecules have the same basic structure.

The overall conformation of the structure is unexpectedly compact when compared with previously determined structures of Lhx3-Isl1 and a related LIM-only complex (*e.g.* Fig. 4*B*) (17, 35). The Lhx4-Isl2 complex has a sharp bend of ~100° at the hinge/spacer region between the two domains. As a result, the two LIM domains of Lhx4 lie almost perpendicular to one another.

Solution Properties of Lhx4-Isl2—SAXS data were measured to probe the structure of Lhx4-Isl2 in solution (supplemental Fig. S3). The linearity of the Guinier plot and the molecular weight of Lhx4-Isl2 estimated from the extrapolated zero-angle scattering ($I(0)$) indicate that under these conditions, the solution contains non-interacting, monodisperse Lhx4-Isl2 molecules (Table 2 and supplemental Fig. S3). The calculated scattering curve from CRYSOL (40) using the coordinates of the Lhx4-Isl2 crystal structure shows deviations from the shape of the experimental curve in the very low-q and mid-q regimes (supplemental Fig. S3). These differences become more pronounced when comparing the interatomic distance distribution functions, $P(r)$, which are very sensitive to symmetry and domain structure and can provide more intuitive information about the shape of a molecule (Fig. 5*A*). The larger radius of gyration, R_g, and longer maximum dimension, D_{max}, of the molecule for the solution data (R_g = 23.5 Å; D_{max} = 75–80 Å) when compared with the crystal structure (R_g = 20.5 Å; D_{max} = 70–75 Å) suggest that the solution structure is more elongated than that in the crystal form.

This type of tandem LIM-binding peptide complex is thought to have some flexibility at the hinge/spacer (17, 41). A rigid body refinement using the crystal structure and the SAXS data was carried out in which the two LIM peptide halves of the crystal structure were allowed to flex at the hinge/spacer. The BUNCH models support a more elongated conformation in solution with an average angle at the hinge/spacer of ~120° (Fig. 5*B*). The more extreme bend in the Lhx4-Isl2 crystal structure likely represents a rarely populated conformation that had a preference for crystallization under the conditions used.

Solution Properties of Lhx3-Isl1 and Lhx3-Isl2—SAXS data were also collected for Lhx3-Isl1, Lhx3-Isl2, and Lhx4-Isl1. The Lhx4-Isl1 sample showed signs of aggregation, and data were not further analyzed (data not shown), but Lhx3-Isl1 and Lhx3-Isl2 were monomers in solution as evidenced by molecular mass estimates from $I(0)$ (Table 2). Lhx3-Isl1 and Lhx3-Isl2 have similar asymmetric $P(r)$ profiles, indicating that the complexes adopted extended conformations in solution (Fig. 5*C*). However, the R_g and D_{max} for Lhx3-Isl2 are shorter (R_g = 22.3 Å; D_{max} ~75 Å) than Lhx3-Isl1(R_g = 26.9 Å; D_{max} ~90 Å), indicating that Lhx3-Isl2 is more compact than its Lhx3-Isl1 counterpart, as seen in the BUNCH models (Fig. 5, *D* and *E*). The solution structural parameters are essentially identical for Lhx3-Isl2 and Lhx4-Isl2 (Fig. 5, *B* and *E*, and supplemental Table S3), suggesting that binding to $Isl2_{LBD}$ causes both Lhx3 and Lhx4 to adopt a more compact structure than does binding to $Isl1_{LBD}$.

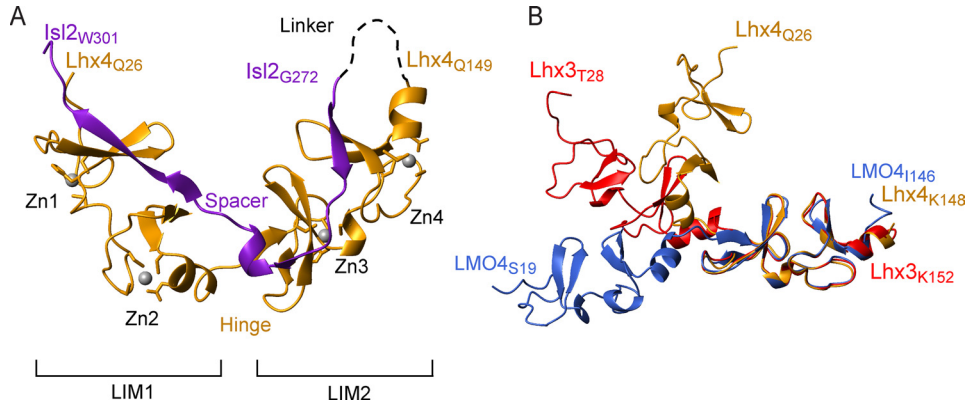

FIGURE 4. **The crystal structure of Lhx4-Isl2.** *A*, ribbon diagram of chain B of the Lhx4-Isl2 complex. Lhx4 is shown in *orange*, and Isl2 is in purple. The position of the linker is shown as a *black dashed line*. *B*, overall shape comparison of tethered LIM homeodomain and LIM-only complexes. Molecules are aligned over the backbone residues of the LIM2 domains of Lhx4-Isl2 (3MMK), Lhx3-Isl1 (2RGT), and LMO4(LIM-only protein 4)$_{LIM1+2}$-Ldb1$_{LID}$ (1RUT) complexes. For clarity, only the LIM domains are shown; Lhx4 is in *orange*, Lhx3 is in *red*, and LMO4 is in *blue*. Images were prepared and alignment of molecules was performed using MolMol (46).

TABLE 2
Structural parameters from small-angle X-ray scattering data

Molecule	Lhx4-Isl2	Lhx3-Isl1	Lhx3-Isl2
D_{max} (Å)	77	89	75
[protein] (mg ml^{-1})	3.10 ± 0.08[a]	5.00 ± 0.11[a]	2.57 ± 0.07[a]
$I(0)$ (cm^{-1})	0.0517 (± 0.0003)[b]	0.0698 (± 0.0003)[b]	0.0400 (± 0.0003)[b]
υ (cm^3 g^{-1})	0.719	0.718	0.720
$\Delta\rho_M$ (× 10^{10} cm^{-2})	2.23	2.24	2.22
R_g (Å)	23.5 (± 0.3)[b]	26.9 (± 0.2)[b]	22.6 (± 0.4)[b]
MM_{exp}[c] (kDa)	20.2 ± 0.5	16.8 ± 0.4	19.0 ± 0.6
MM_{pr} (kDa)	18.9	19.0	18.8
MM_{exp}/MM_{pr}	1.07	0.88	1.01

[a] Error is 1 S.D.
[b] $I(0)$ and R_g were derived from $P(r)$ using GIFT. The errors for these values were obtained by analyzing the Guinier region of the scattering in PRIMUS. GIFT does not produce errors for these values.
[c] $MM_{exp} = I(0)N_A/[protein]\Delta\rho_M{}^2$.

Overall these solution scattering studies (see supplemental data 3 for a detailed analysis) indicate that tethered Lhx3/4-Isl1/2 complexes are likely to exist as an ensemble of elongated complexes with some flexibility at the hinge/spacer. Although the molecular details of each LIM domain peptide module are unlikely to be affected by flexion, details concerning the hinge/spacer regions will likely vary between members of the ensembles, and analyses of high resolution structure should be careful not to overinterpret details from these regions.

Identifying Binding Hotspots in Lhx3/4·Isl1/2 Complexes—We used yeast two-hybrid analysis to compare the ability of the individual LIM domains from Lhx3 and Lhx4 to interact with Isl1$_{LBD}$, Isl2$_{LBD}$, and Ldb1$_{LID}$ (supplemental Table S4) (17). The LIM2 domains from Lhx3 and Lhx4 were both capable of independently interacting with Isl1$_{LBD}$ and Ldb1$_{LID}$, whereas the LIM1 domains could bind weakly to Ldb1$_{LID}$ (some yeast growth was evident only under low stringency selection conditions), but not to Isl1$_{LBD}$. No individual LIM domain from either Lhx3 or Lhx4 showed evidence of an interaction with Isl2$_{LBD}$ in this assay.

The Lhx3-binding domains of Isl1 and Isl2 were subjected to mutagenesis to identify the key residues in those domains that mediate binding with Lhx3 and Lhx4. Residues were mutated to alanine (or glycine if the native residue was alanine). Initially sequential sets of three consecutive residues were mutated and tested for their ability to interact with the LIM domains from Lhx3 and Lhx4 using yeast two-hybrid analysis. For those triple mutants that showed significantly reduced levels of binding, a second round of single point mutants was generated and tested in the same manner. The results from these mutagenic screens are reported in supplemental data 4 and are summarized in Fig. 6*A*. Finally, two point mutants, Isl1$_{M265L}$ and Isl2$_{L275M}$, were used to test binding specificity (Fig. 6*B* and supplemental data 4).

Mutations in the N-terminal (and not the C-terminal) half of Isl1$_{LBD}$ significantly disrupted binding to both Lhx3 and Lhx4 (Fig. 6*A*) (17), which is consistent with only the LIM2 domains from the Lhx proteins being able to independently bind Isl1$_{LBD}$. In contrast, mutations in both the N-terminal and the C-terminal halves of Isl2$_{LBD}$ abrogated binding to Lhx3 and Lhx4 (Fig. 6*A*), consistent with both LIM domains of the Lhx proteins being required to mediate an interaction with Isl2$_{LBD}$.

Among the residues identified as being most important for the interactions, Isl1$_{265-267}$, and Isl2$_{275-277/293-295}$, the only sequence difference between the two paralogues is a conservative switch from Met-265 in Isl1 to Leu-275 in Isl2. Interaction data for Isl1$_{M265L}$ and Isl2$_{L275M}$ suggest that although Lhx3 has no apparent preference for either residue at Isl1$_{265}$/Isl2$_{275}$, Lhx4 binds with higher affinity when there is a methionine at this position (Fig. 6*B*, supplemental Fig. S4, and supplemental Table S4).

Relative Stabilities of Lhx-Isl Complexes—We used an indirect approach to probe the relative binding affinities of Lhx3 and Lhx4 for each of Isl1 and Isl2. Stable forms of isolated LIM domains from Lhx3 and Lhx4 cannot be produced in a recom-

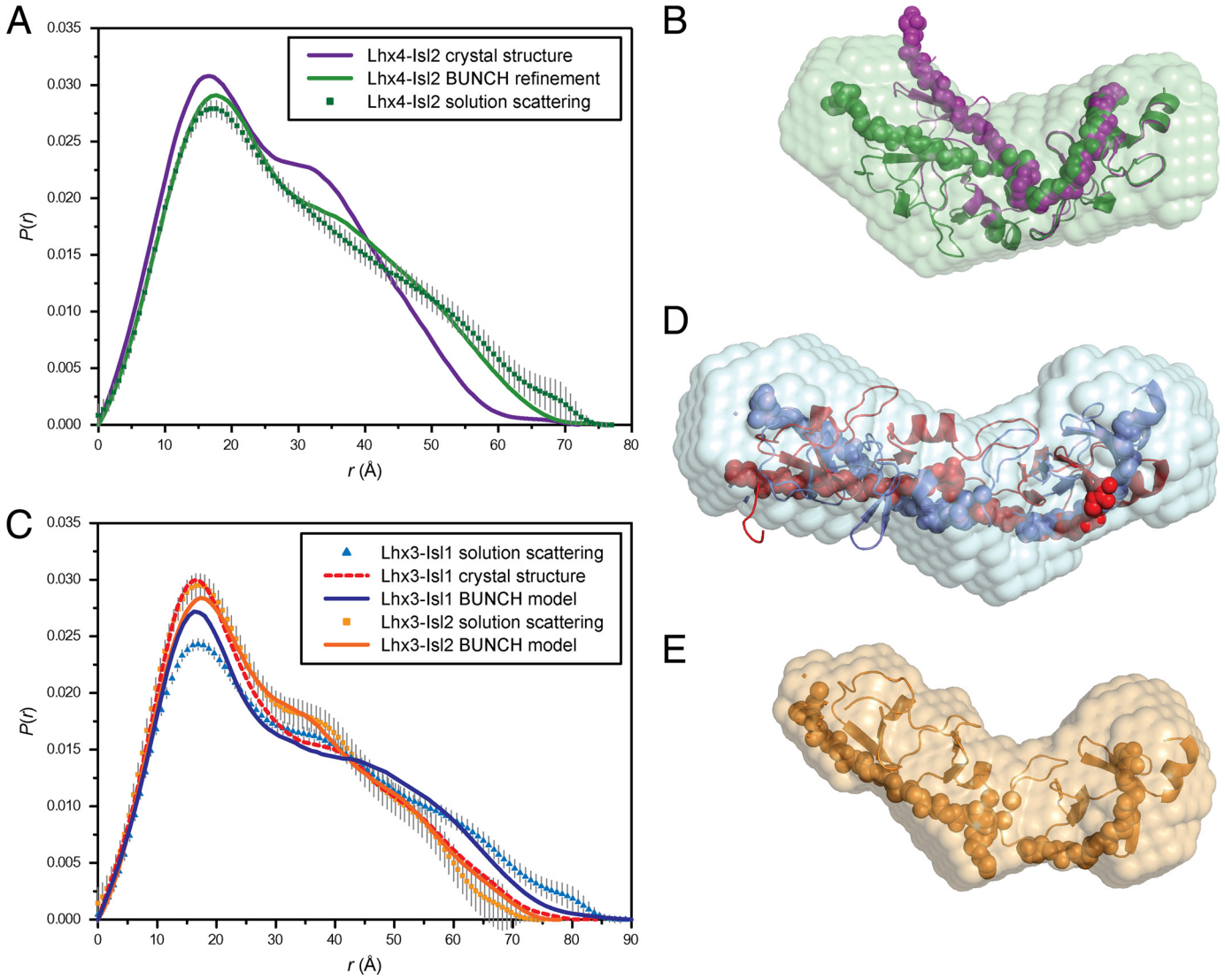

FIGURE 5. **The solution structures of Lhx3/4-Isl1/2.** *A*, *P*(*r*) profiles from experimental scattering data for Lhx4-Isl2 (*green squares*) and calculated scattering profiles from the Lhx4-Isl2 crystal structure (*purple line*) and the generated BUNCH model (*green line*). *B*, alignment using the atoms of $Lhx4_{LIM2}$ of the Lhx4-Isl2 crystal structure (*purple*) with the best-fit BUNCH model (*green*) and *ab initio* DAMMIF reconstruction (*transparent green surface*). *C*, *P*(*r*) profiles from experimental scattering data for Lhx3-Isl1 (*blue triangles*) and Lhx3-Isl2 (*orange squares*) and calculated scattering profiles from the Lhx3-Isl1 crystal structure (*red dashed line*), the Lhx3-Isl1 BUNCH model (*dark blue line*), and the Lhx3-Isl2 BUNCH model (*dark orange line*). *D*, alignment using the atoms of $Lhx3_{LIM2}$ of the Lhx3-Isl1 crystal structure (*red*) with the best-fit BUNCH model (*blue*) and *ab initio* DAMMIF reconstruction (*transparent blue surface*). *E*, the best-fit BUNCH model (*orange*) and *ab initio* DAMMIF reconstruction (*transparent orange surface*) for Lhx3-Isl2. LIM domains are shown as *ribbons*, and LBDs as are shown as *spheres*.

binant fashion, preventing the use of standard binding experiments (such as ELISA, isothermal titration calorimetry, or surface plasmon resonance). We instead compared the relative resistance of the Lhx3/4-Isl1/2 complexes to chemical denaturation, an approach previously used to gauge the relative stability of tethered Lhx3-Isl1 and $Lhx3_{LIM1+2}$-$Ldb1_{LID}$ complexes (17). The LBD/LID peptides are largely unstructured, and if we only compare identical folded LIM domains, the differences in resistance to chemical denaturation should report on differences in binding affinity between the LIM domains and the peptides. As the sequences of $Lhx3_{LIM1+2}$ and $Lhx4_{LIM1+2}$ differ, we only compared the apparent stability of Lhx3-Isl1 with Lhx3-Isl2, or Lhx4-Isl1 with Lhx4-Isl2, and did not compare Lhx3 constructs with Lhx4 constructs. Note that these proteins do not exhibit reversible unfolding, meaning that the data cannot be used to calculate differences in free energy of unfolding and/or actual binding affinities.

The resistance of the constructs to denaturation was measured by monitoring the change in λ_{max} of tryptophan fluorescence as a function of guanidine hydrochloride concentration. Lhx3-Isl1 and Lhx3-Isl2 tethered complexes had virtually identical unfolding curves, with a midpoint of unfolding at ~2 M guanidine hydrochloride, suggesting that the Lhx3-Isl1 and Lhx3-Isl2 complexes have the same apparent stability (Fig. 6*C*). In contrast, Lhx4-Isl1 showed a midpoint of unfolding at ~2.5 M when compared with ~2 M for Lhx4-Isl2, suggesting that the Lhx4-Isl1 tethered complex is probably more stable than the Lhx4-Isl2 complex (Fig. 6*D*).

DISCUSSION

We have now shown that an Lhx3-binding domain exists in Isl2 as well as Isl1 and that both of these domains can bind to each of Lhx3 and Lhx4. Overall Lhx3 and Lhx4 share 66% sequence identity, whereas Isl1 and Isl2 share 74% sequence

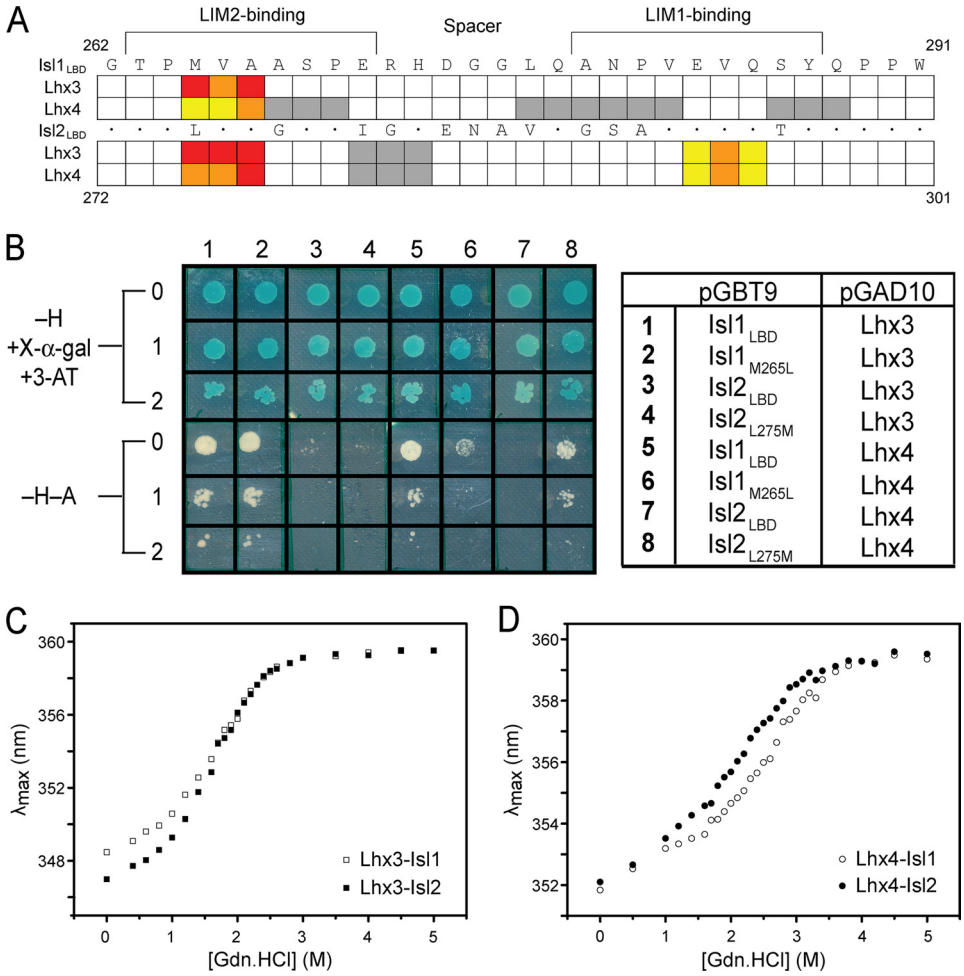

FIGURE 6. **Binding and apparent stability in Lhx3/4·Isl1/2 complexes.** *A*, summary of alanine mutagenic screening assayed by yeast two-hybrid analysis from supplemental Table S4. The sequence of $Isl1_{LBD}$ (262–291) is shown. The sequence of $Isl2_{LBD}$ (272–301) shows where residues are conserved (*) or different. *Colored boxes* indicate where mutation had a strong (*red*), moderate (*orange*), or minor effect (*yellow*). *White boxes* indicate residues mutated in triple-alanine constructs that had a minor effect on growth of yeast. *Gray boxes* indicate no effect on yeast growth. *B*, comparison of wild-type and mutant LBDs from Isl1/Isl2 binding to the LIM domains of Lhx3/Lhx4 by yeast two-hybrid analysis. AH109 yeast cells co-transformed with pGBT9/pGAD10 vectors shown on the *right* were tested for growth under different selection conditions (−H + X-α-gal + 3-AT) or (−H−A); *0* indicates no dilution of yeast cells ($A_{600\ nm} = 0.2$), *1* indicates a 1:10 dilution ($A_{600\ nm} = 0.02$), and *2* indicates a 1:100 dilution ($A_{600\ nm} = 0.002$). *C*, resistance of Lhx3-Isl1/2 complexes to denaturation by guanidine hydrochloride (*Gdn.HCl*). □, Lhx3-Isl1; ■, Lhx3-Isl2. *D*, resistance of Lhx4-Isl1/2 complexes to denaturation by guanidine hydrochloride. ○, Lhx4-Isl1; ●, Lhx4-Isl2. For *C* and *D*, λ_{max} reports maximum emission wavelength in the range 320–380 nm with excitation at 295 nm.

identity, which is highest in the homeodomains (95 and 98% sequence identity, respectively) and LIM domains (83 and 82% identity, respectively). $Isl1_{LBD}$ and $Isl2_{LBD}$ have lower sequence identity (60%). The structure of the Lhx4-Isl2 complex reported here is most divergent in sequence from the existing Lhx3-Isl1 complex structure (17), allowing a structure-guided interpretation of sequence, binding, and mutational data for Lhx3/Lhx4 and Isl1/Isl2 interactions.

The Lhx3-Isl1 and Lhx4-Isl2 Structures Have Similar Overall Structures—The overall shapes of Lhx3-Isl1 and Lhx4-Isl2 from the crystal structures differ by the angles at the hinge/spacer (~100° for Lhx4-Isl2 and ~165° for Lhx3-Isl1; Fig. 4*B*). The solution structural parameters derived from SAXS data indicate that, although this difference is exaggerated in the crystal forms, in solution there is a difference in the hinge/spacer angles between the two complexes such that Lhx4-Isl2 and Lhx3-Isl2 are more compact than Lhx3-Isl1 (have a smaller angle). At the domain level, the folds of the LIM domains of Lhx3 and Lhx4 are highly conserved. An alignment of the backbone atoms from chain B of the Lhx4-Isl2 structure and the Lhx3-Isl1 structure (Protein Data Bank (PDB) accession code 2RGT, chain B; Ref. 17) gives an r.m.s.d. of 0.77 Å for the LIM1 domains (Fig. 7*A*) and 0.59 Å for the LIM2 domains (Fig. 7*B*).

$Isl1_{LBD}$ and $Isl2_{LBD}$ have a backbone r.m.s.d. of 8.7 Å, which is not surprising given the different shapes of the complexes. If we consider the LIM1- and LIM2-binding regions of the LBDs separately, the r.m.s.d. drops to 0.56 Å for $Isl1_{279-287}$/$Isl2_{289-297}$ and 0.38 Å for $Isl1_{262-273}$/$Isl2_{272-283}$. $Isl2_{LBD}$ forms four well defined β-strands at the interface with Lhx4, and $Isl1_{LBD}$ shows an almost identical binding topology, with three well defined strands and evidence of a fourth short β-strand from two inter-domain backbone-backbone hydrogen bonds over the third zinc-coordinating module of Lhx3. The program PISA (42) reveals similar surface areas buried at the interfaces of the two complexes, ~1490 $Å^2$ for $Lhx3_{LIM1+2}$·$Isl1_{LBD}$ and ~1540 $Å^2$ for $Lhx4_{LIM1+2}$·$Isl2_{LBD}$.

Structure-guided Interpretation of Binding Data—A comparison of the interfaces in the two structures shows that there is a

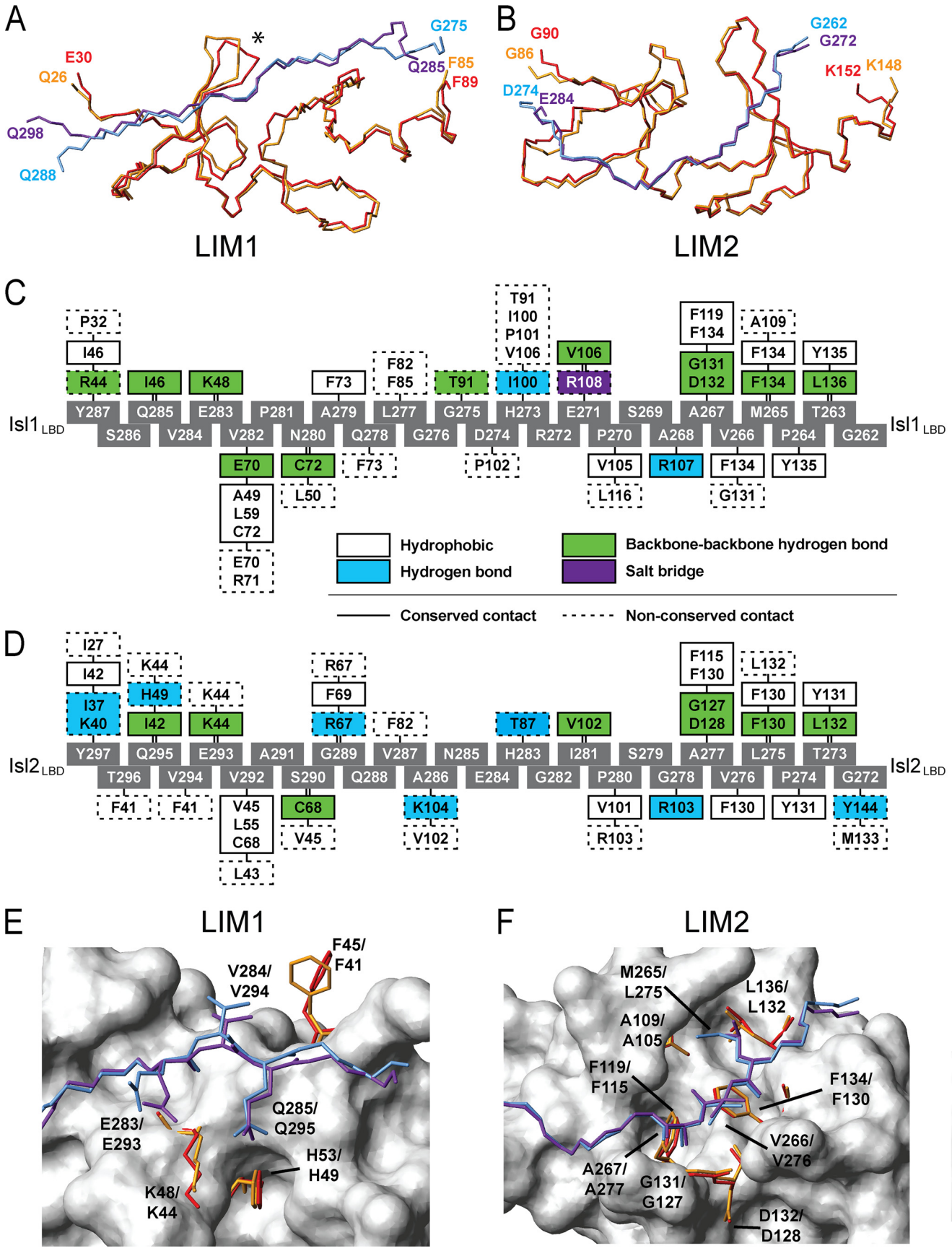
A
E30
Q26
Q298
Q288
G275
Q285
F85
F89
LIM1
B
G90
G86
D274
E284
G262
G272
K152
K148
LIM2
C
P32
I46
R44
I46
K48
F73
F82
F85
T91
T91
I100
P101
V106
V106
R108
F119
F134
G131
D132
A109
F134
F134
Y135
L136
Isl1 LBD
Y287
Q285
E283
P281
A279
L277
G275
H273
E271
S269
A267
M265
T263
S286
V284
V282
N280
Q278
G276
D274
R272
P270
A268
V266
P264
G262
Isl1 LBD
E70
C72
F73
P102
V105
R107
F134
Y135
A49
L59
C72
L50
L116
G131
E70
R71
Hydrophobic
Backbone-backbone hydrogen bond
Hydrogen bond
Salt bridge
Conserved contact
Non-conserved contact
D
I27
I42
I37
K40
K44
H49
I42
K44
K44
R67
F69
R67
F82
T87
V102
F115
F130
G127
D128
L132
F130
F130
Y131
L132
Isl2 LBD
Y297
Q295
E293
A291
G289
V287
N285
H283
I281
S279
A277
L275
T273
T296
V294
V292
S290
Q288
A286
E284
G282
P280
G278
V276
P274
G272
Isl2 LBD
F41
F41
V45
L55
C68
L43
C68
V45
K104
V102
V101
R103
R103
F130
Y131
Y144
M133
E
LIM1
V284/
V294
F45/
F41
E283/
E293
Q285/
Q295
H53/
H49
K48/
K44
F
LIM2
M265/
L275
L136/
L132
A109/
A105
F119/
F115
F134/
F130
V266/
V276
A267/
A277
G131/
G127
D132/
D128

high sequence similarity in the stretches of the LBDs that contact each LIM domain (the binding motifs) but poor sequence conservation in and around the spacer (Fig. 6*A*). The specific intermolecular contacts of the two complexes are almost identical at the LIM2/N-terminal LBD interfaces but are more varied at the LIM1/C-terminal LBD interfaces (Fig. 7, *C* and *D*). In the latter region, there are minor variations in the side-chain conformations of some residues at the interface when compared with those at the LIM2/N-terminal LBD interfaces (Fig. 7, *E* and *F*). These differences in structure are reflected by different contributions to binding of the C-terminal halves of $Isl1_{LBD}$ and $Isl2_{LBD}$ and the effects of mutation on binding.

$Isl2_{E293A/V294A/Q295A}$ abrogated binding to both Lhx3 and Lhx4 (Fig. 6*A*, supplemental Fig. S4, and supplemental Table S4). $Isl2_{E293\text{-}Q295}$ is equivalent to $Isl1_{E283\text{-}Q285}$ in Isl1, but the side chains of those residues form predominantly different sets of contacts in the two complexes (Fig. 7, *C* and *D*), and the backbone alignment of Lhx3 and Lhx4 in this region shows more deviation than elsewhere in the molecules (Fig. 7*A*, marked by an *asterisk*). The side-chain conformations of $Isl2_{E293}$ and $Isl2_{Q295}$ and the residues that they contact, $Lhx4_{F41}$ and $Lhx4_{K44}$, also differ from those of the corresponding residues in the Lhx3-Isl1 structure (Fig. 7*E*). Although these differences are mostly subtle, the changes appear significant when compared with the N-terminal halves of the $Isl1_{LBD}$ and $Isl2_{LBD}$, where sets of contacts and side-chain conformations are almost identical (*e.g.* Fig. 7, *C*, *D*, and *F*), even in non-conserved residues.

The essentially identical solution parameters for Lhx3-Isl2 and Lhx4-Isl2, coupled with the same patterns of binding of $Isl2_{LBD}$ for Lhx3 and Lhx4 (which differ from the $Isl1_{LBD}$ patterns for the same targets), imply that the binding of $Isl2_{LBD}$ results in a different conformation in Lhx3 and Lhx4 than does $Isl1_{LBD}$. That is, although the mutation to alanine of residues in the LBD spacers does not appear to significantly affect binding, sequence variation in the spacers and the minor differences in the binding motifs induce different angles at the hinge/spacer. These differences might influence the formation of higher order complexes involving these protein pairs to regulate different activities in cells by creating or obscuring binding sites.

The chemical denaturation data for Lhx4 tethered complexes indicate that Lhx3-Isl1 and Lhx3-Isl2 have the same resistance to denaturation, but Lhx4-Isl2 is less resistant than Lhx4-Isl1. This difference may reflect an increased binding affinity of Lhx4·Isl1 over Lhx4·Isl2; however, thermodynamic binding data, which have thus far not been possible to obtain, would be required to establish whether this is the case. A small increase in the apparent affinity of Lhx4 (but not Lhx3) for the equivalent Isl1 residue and a decreased apparent affinity for the Isl2 residue at position $Isl1_{M265}$/$Isl2_{L275}$ (Fig. 6*B*, supplemental Fig. S4, and supplemental Table S4) implies that although Lhx3·Isl1 and Lhx3·Isl2 are interchangeable in terms of binding specificity, Lhx4 appears to have a small preference for binding Isl1 over Isl2.

Redundancy and Divergence of LIM Homeodomain Proteins—Paralogous pairs of genes are often thought to have arisen via genome duplication events. As demonstrated by their different knock-out phenotypes in mice, the pairs Lhx3/Lhx4 and Isl1/Isl2 have diverged in some of their functions, but all four proteins are expressed in postmitotic ventral motor neurons (43). Lhx3 and Lhx4 are apparently redundant in those cells as mice embryos in which either Lhx3 or Lhx4 is knocked out have normal ventral motor neurons (5). In addition, human Lhx3 mutations that cause combined pituitary hormone deficiency syndrome do not cause motor neuron abnormalities (44). It is only when both Lhx3 and Lhx4 are knocked out that ventral motor neurons fail to develop (5). Although at least some expression of Isl2 is required for all of the motor neuron subtypes to develop, Isl2 appears to act by increasing levels of Islet activity rather than providing a separate function (9, 11). Indeed, either Isl1 or Isl2 can effectively promote ectopic motor neuron differentiation when co-expressed with Lhx3, suggesting that the Islet proteins do have the same molecular function in this context (9–12). If Lhx4 does bind Isl2 less strongly than it does Isl1, co-expression of Isl2 with Lhx4 rather than Lhx3 should show a reduction in the efficiency of motor neuron development.

It seems likely that conservation of function of Lhx3/Lhx4 and Isl1/Isl2 in motor neurons represents a co-evolutionary process; high levels of Lhx3/Lhx4 must be matched by high levels of Islet proteins to achieve the correct balance of cell-specific transcription complexes. However, the presence of four possible pairwise complexes indicates a highly redundant system that could accommodate evolutionary divergence; simultaneous disruptions to both Lhx3 and Isl1 would probably be required to severely compromise motor neuron development. Teleost fish have higher numbers of LIM homeodomain (and many other) genes than other vertebrates, most likely from additional genome duplication events. The sequences of LBDs from the Islet proteins of these fish suggest the presence of a single Isl1 paralogue, with two or more proteins that are Isl2-like (or more divergent in sequence), suggesting that the duplicated genes are acquiring more diverse functions.

Divergence is also evident in apparent differences in the way that Isl1 and Isl2 mediate binding to the Lhx3 and Lhx4 targets. Solution scattering data indicate that Isl2 induces a more compact structure (smaller angle at the hinge/spacer) in Lhx3 and Lhx4 than does Isl1 (Fig. 5), probably due to differences in con-

FIGURE 7. **Comparison of Lhx3/4·Isl1/2 interaction interfaces.** *A* and *B*, backbone alignment of Lhx3 (*red*) and Lhx4 (*orange*) using the LIM1 (*A*) and LIM2 (*B*) domains. The backbones of Isl1 (*blue*) and Isl2 (*purple*) are also shown. An *asterisk* indicates loops in Lhx3/Lhx4 that show the most variation in the backbone alignment. *C* and *D*, interaction maps indicating the residues from Lhx3-Isl1 (*C*) and Lhx4-Isl2 (*D*) that make contacts as identified by LIGPLOT (47). *Gray boxes* are residues of $Isl1_{LBD}$ or $Isl2_{LBD}$. *Colored boxes* for the Lhx residues define the type of interaction as indicated; *solid lines* represent conserved contacts between the two complexes, and *dashed lines* indicate non-conserved contacts between the two complexes. Note that the numbering between Lhx3 and Lhx4 differs by four (*e.g.* $Lhx4_{F130}$ corresponds to $Lhx3_{F134}$) and by 10 between Isl1 and Isl2 (*e.g.* $Isl1_{M265}$ corresponds to $Isl2_{L275}$). *E* and *F*, the key residues in the two complexes from Lhx3 and Lhx4 LIM1 domains (*E*) and Lhx3 and Lhx4 LIM2 domains (*F*). The side chains of critical residues from Isl1 (*blue*) and Isl2 (*purple*) identified using yeast two-hybrid analysis and the residues they contact are shown (Lhx3 in *red* and Lhx4 in *orange*), as well as the backbone atoms of non-critical residues from $Isl1_{LBD}$ and $Isl2_{LBD}$. Non-Isl-binding residues from $Lhx4_{LIM1}$ and $Lhx4_{LIM2}$ are shown in surface representation (*white*). The residues $Isl1_{M265}$ and $Isl2_{L275}$ adopt equivalent rotamers, *mtp* and *mt*, respectively.

tacts between hinge and spacer residues (Fig. 7, *C* and *D*). The C-terminal half of $Isl2_{LBD}$ appears to make a larger contribution to binding than the same region of Isl1. Despite these different binding patterns, $Isl1_{LBD}$ and $Isl2_{LBD}$ appear to have equivalent affinities for Lhx3 (Fig. 6*B*), suggesting that the N-terminal half of Isl2 makes a correspondingly weaker contribution to binding. However, although these complexes combine modular interactions between the LIM domains and cognate peptide sequences to result in high affinity complexes, the interaction affinities of the modules may not be additive, as suggested by data for LIM-only protein 2 (41, 45). Differences in binding at the two domains could play a role in the kinetics of exchange of partners between different transcription complexes that contain LIM homeodomain and LIM-only proteins (17).

In conclusion, our studies have shown that although the pairwise interactions between the paralogous pairs of LIM homeodomain proteins Lhx3/Lhx4 and Isl1/Isl2 have many similarities that explain high levels of redundancy in motor neuron development, minor differences are evident that reflect evolutionary divergence for these proteins in other developmental pathways.

Acknowledgment—We thank Don Parkin for collection and preliminary evaluation of SAXS data.

REFERENCES

1. Matthews, J. M., Bhati, M., Lehtomaki, E., Mansfield, R. E., Cubeddu, L., and Mackay, J. P. (2009) *Curr. Pharm. Des.* **15,** 3681–3696
2. Bachy, I., Failli, V., and Rétaux, S. (2002) *Neuroreport* **13,** A23–A27
3. Tsuchida, T., Ensini, M., Morton, S. B., Baldassare, M., Edlund, T., Jessell, T. M., and Pfaff, S. L. (1994) *Cell* **79,** 957–970
4. Failli, V., Rogard, M., Mattei, M. G., Vernier, P., and Rétaux, S. (2000) *Genomics* **64,** 307–317
5. Sharma, K., Sheng, H. Z., Lettieri, K., Li, H., Karavanov, A., Potter, S., Westphal, H., and Pfaff, S. L. (1998) *Cell* **95,** 817–828
6. Li, H., Witte, D. P., Branford, W. W., Aronow, B. J., Weinstein, M., Kaur, S., Wert, S., Singh, G., Schreiner, C. M., Whitsett, J. A., *et al.* (1994) *EMBO J.* **13,** 2876–2885
7. Sheng, H. Z., Zhadanov, A. B., Mosinger, B., Jr., Fujii, T., Bertuzzi, S., Grinberg, A., Lee, E. J., Huang, S. P., Mahon, K. A., and Westphal, H. (1996) *Science* **272,** 1004–1007
8. Pfaff, S. L., Mendelsohn, M., Stewart, C. L., Edlund, T., and Jessell, T. M. (1996) *Cell* **84,** 309–320
9. Thaler, J. P., Koo, S. J., Kania, A., Lettieri, K., Andrews, S., Cox, C., Jessell, T. M., and Pfaff, S. L. (2004) *Neuron* **41,** 337–350
10. Hutchinson, S. A., and Eisen, J. S. (2006) *Development* **133,** 2137–2147
11. Song, M. R., Sun, Y., Bryson, A., Gill, G. N., Evans, S. M., and Pfaff, S. L. (2009) *Development* **136,** 2923–2932
12. Thaler, J. P., Lee, S. K., Jurata, L. W., Gill, G. N., and Pfaff, S. L. (2002) *Cell* **110,** 237–249
13. Jurata, L. W., and Gill, G. N. (1997) *Mol. Cell. Biol.* **17,** 5688–5698
14. Jurata, L. W., Kenny, D. A., and Gill, G. N. (1996) *Proc. Natl. Acad. Sci. U.S.A.* **93,** 11693–11698
15. van Meyel, D. J., O'Keefe, D. D., Jurata, L. W., Thor, S., Gill, G. N., and Thomas, J. B. (1999) *Mol Cell* **4,** 259–265
16. Agulnick, A. D., Taira, M., Breen, J. J., Tanaka, T., Dawid, I. B., and Westphal, H. (1996) *Nature* **384,** 270–272
17. Bhati, M., Lee, C., Nancarrow, A. L., Lee, M., Craig, V. J., Bach, I., Guss, J. M., Mackay, J. P., and Matthews, J. M. (2008) *EMBO J.* **27,** 2018–2029
18. Bhati, M., Lee, M., Nancarrow, A. L., Bach, I., Guss, J. M., and Matthews, J. M. (2008) *Acta Crystallogr. Sect. F Struct. Biol. Cryst. Commun.* **64,** 297–299
19. Gadd, M. S., Langley, D. B., Guss, J. M., and Matthews, J. M. (2009) *Acta Crystallogr. Sect. F Struct. Biol. Cryst. Commun.* **65,** 151–153
20. Deane, J. E., Mackay, J. P., Kwan, A. H., Sum, E. Y., Visvader, J. E., and Matthews, J. M. (2003) *EMBO J.* **22,** 2224–2233
21. Cross, A. J., Jeffries, C. M., Trewhella, J., and Matthews, J. M. (2010) *J. Mol. Biol.* **399,** 133–144
22. Terwilliger, T. C., and Berendzen, J. (1999) *Acta Crystallogr. D. Biol. Crystallogr.* **55,** 849–861
23. Terwilliger, T. C. (2000) *Acta Crystallogr. D. Biol. Crystallogr.* **56,** 965–972
24. Emsley, P., and Cowtan, K. (2004) *Acta Crystallogr. D Biol. Crystallogr.* **60,** 2126–2132
25. Winn, M. D., Isupov, M. N., and Murshudov, G. N. (2001) *Acta Crystallogr. D Biol. Crystallogr.* **57,** 122–133
26. Murshudov, G. N., Vagin, A. A., and Dodson, E. J. (1997) *Acta Crystallogr. D Biol. Crystallogr.* **53,** 240–255
27. Adams, P. D., Grosse-Kunstleve, R. W., Hung, L. W., Ioerger, T. R., McCoy, A. J., Moriarty, N. W., Read, R. J., Sacchettini, J. C., Sauter, N. K., and Terwilliger, T. C. (2002) *Acta Crystallogr. D Biol. Crystallogr.* **58,** 1948–1954
28. Lovell, S. C., Davis, I. W., Arendall, W. B., 3rd, de Bakker, P. I., Word, J. M., Prisant, M. G., Richardson, J. S., and Richardson, D. C. (2003) *Proteins* **50,** 437–450
29. Jeffries, C. M., Whitten, A. E., Harris, S. P., and Trewhella, J. (2008) *J. Mol. Biol.* **377,** 1186–1199
30. Orthaber, D., Bergmann, A., and Glatter, O. (2000) *J. Appl. Crystallogr.* **33,** 218–225
31. Whitten, A. E., Cai, S. Z., and Trewhella, J. (2008) *J. Appl. Crystallogr.* **41,** 222–226
32. Konarev, P. V., Volkov, V. V., Sokolova, A. V., Koch, M. H., and Svergun, D. I. (2003) *J. Appl. Crystallogr.* **36,** 1277–1282
33. Petoukhov, M. V., and Svergun, D. I. (2005) *Biophys. J.* **89,** 1237–1250
34. Svergun, D. I. (1992) *J. Appl. Crystallogr.* **25,** 495–503
35. Deane, J. E., Ryan, D. P., Sunde, M., Maher, M. J., Guss, J. M., Visvader, J. E., and Matthews, J. M. (2004) *EMBO J.* **23,** 3589–3598
36. Jeffries, C. M., Graham, S. C., Stokes, P. H., Collyer, C. A., Guss, J. M., and Matthews, J. M. (2006) *Protein Sci.* **15,** 2612–2618
37. Deane, J. E., Sum, E., Mackay, J. P., Lindeman, G. J., Visvader, J. E., and Matthews, J. M. (2001) *Protein Eng.* **14,** 493–499
38. Lee, C., Nancarrow, A. L., Bach, I., Mackay, J. P., and Matthews, J. M. (2005) *J. Biomol. NMR* **33,** 198
39. Deane, J. E., Maher, M. J., Langley, D. B., Graham, S. C., Visvader, J. E., Guss, J. M., and Matthews, J. M. (2003) *Acta Crystallogr. D Biol. Crystallogr.* **59,** 1484–1486
40. Svergun, D., Barberato, C., and Koch, M. H. (1995) *J. Appl. Crystallogr.* **28,** 768–773
41. El Omari, K., Hoosdally, S. J., Tuladhar, K., Karia, D., Vyas, P., Patient, R., Porcher, C., and Mancini, E. J. (2011) *Blood* **117,** 2146–2156
42. Krissinel, E., and Henrick, K. (2007) *J. Mol. Biol.* **372,** 774–797
43. Tanabe, Y., William, C., and Jessell, T. M. (1998) *Cell* **95,** 67–80
44. Netchine, I., Sobrier, M. L., Krude, H., Schnabel, D., Maghnie, M., Marcos, E., Duriez, B., Cacheux, V., Moers, A., Goossens, M., Grüters, A., and Amselem, S. (2000) *Nat. Genet.* **25,** 182–186
45. Ryan, D. P., Sunde, M., Kwan, A. H., Marianayagam, N. J., Nancarrow, A. L., Vanden Hoven, R. N., Thompson, L. S., Baca, M., Mackay, J. P., Visvader, J. E., and Matthews, J. M. (2006) *J. Mol. Biol.* **359,** 66–75
46. Koradi, R., Billeter, M., and Wüthrich, K. (1996) *J. Mol. Graph.* **14,** 51–55
47. Wallace, A. C., Laskowski, R. A., and Thornton, J. M. (1995) *Protein Eng.* **8,** 127–134